Editors' Suggestion   Featured in Physics

Voltage-Controlled Magnon Transistor via Tuning Interfacial Exchange Coupling

Y. Z. Wang [1,2] T. Y. Zhang,[1] J. Dong,[1] P. Chen,[1] G. Q. Yu,[1,3] C. H. Wan,[1,3,*] and X. F. Han [1,2,3,†]

[1]*Beijing National Laboratory for Condensed Matter Physics, Institute of Physics, University of Chinese Academy of Sciences, Chinese Academy of Sciences, Beijing 100190, China*

[2]*Center of Materials Science and Optoelectronics Engineering, University of Chinese Academy of Sciences, Beijing 100049, China*

[3]*Songshan Lake Materials Laboratory, Dongguan, Guangdong 523808, China*

Magnon transistors that can effectively regulate magnon transport by an electric field are desired for magnonics, which aims to provide a Joule-heating free alternative to the conventional electronics owing to the electric neutrality of magnons (the key carriers of spin-angular momenta in the magnonics). However, also due to their electric neutrality, magnons have no access to directly interact with an electric field and it is thus difficult to manipulate magnon transport by voltages straightforwardly. Here, we demonstrated a gate voltage (V_g) applied on a nonmagnetic metal and magnetic insulator (MI) interface that bent the energy band of the MI and then modulated the probability for conduction electrons in the nonmagnetic metal to tunnel into the MI, which can consequently enhance or weaken the spin-magnon conversion efficiency at the interface. A voltage-controlled magnon transistor based on the magnon-mediated electric current drag (MECD) effect in a Pt-$Y_3Fe_5O_{12}$-Pt sandwich was then experimentally realized with V_g modulating the magnitude of the MECD signal. The obtained efficiency (the change ratio between the MECD voltage at $\pm V_g$) reached $10\%/(MV/cm)$ at 300 K. This prototype of magnon transistor offers an effective scheme to control magnon transport by a gate voltage.

DOI: 10.1103/PhysRevLett.132.076701

Magnons as the collective excitation of a magnetically ordered lattice possessing both spin-angular momenta and phases but no charges [1], become an ideal information carrier for the Joule-heating-free electronics [2,3]. In order to efficiently manipulate magnon transport, magnon transistors, as an elementary brick for magnonics, have long been desired. Despite great achievements in efficiently exciting [4–10], propagating [11–13], and detecting [14–18] magnons, the electric neutrality of magnons sets a high level of difficulty in controlling magnon transport by electric fields.

Several magnon gating methods have been realized. The $Y_3Fe_5O_{12}$(YIG)-Au-YIG-Pt magnon valves [19] and YIG-NiO-YIG-Pt magnon junctions [20–22] are gated by an external magnetic field (**H**). Large (small) spin-Seebeck voltage was output by setting the two YIG layers into the parallel (antiparallel) state by **H** currently, though spin-orbit torques are potentially used to gate the magnon valves and junctions in the future [23]. Another magnon-spin valve YIG-CoO-Co was also **H**-gateable [24]. Its spin pumping voltage depends on the **H**-controlled parallel and antiparallel states between YIG and Co. Another method is gating current. In the magnon transistor consisting of three Pt stripes on top of a YIG film [25], a charge current in the leftmost Pt stripe excites a magnon current in YIG via (i) the spin Hall effect in Pt and (ii) the interfacial s-d coupling at the Pt-YIG interface. The as-induced magnon

current diffuses toward the rightmost Pt stripe where the inverse process occurs, resulting in a detectable voltage. This phenomenon, featured by the nonlocal electric induction across a MI with the help of incoherent thermal magnons (with energies $hf \lesssim k_BT$), is named as the magnon-mediated electric current drag (MECD) effect [4,6]. A gating current flowing in the middle Pt strip changes magnon density of YIG in the gate region and consequently modifies the MECD efficiency.

Microwave assisted gating [26–28], magnetization switching assisted gating [29–31] and nanostructures gating [32–34] have been demonstrated in magnonic devices based on metallic ferromagnets. However, due to no direct coupling of magnons with any electric fields, magnon transistors inherently controlled by a gate voltage (V_g), a desired manner advantageous in energy consumption and convenience, are still missing.

Inspired by the model of Chen *et al.* [35,36], we realize the spin-mixing conductance ($G_{\uparrow\downarrow}$) at a nonmagnetic metal and metallic insulator (NM-MI) interface relies sensitively on the interfacial s-d exchange coupling. Here, we proposed a voltage-controlled magnon transistor. The input channel corresponds to the dc current applied on the bottom NM electrode; the output signal corresponds to the dc current generated on the top NM electrode or the induced voltage in an open circuit condition; and the gating mechanism is achieved through the voltage applied on
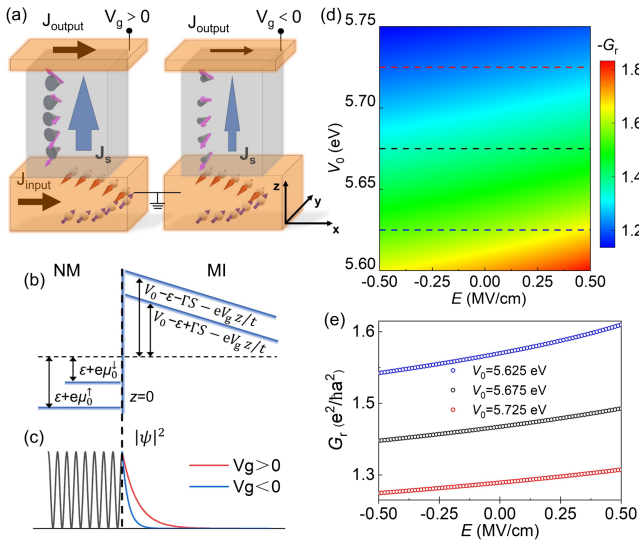
FIG. 1. Mechanism of voltage-gated magnon transistor. (a) Schematics of the voltage-gated magnon transistor. A spin current is generated by the spin Hall effect in the bottom NM, which induces imbalanced spin accumulation (μ_s) at the bottom NM-MI interface. Because of the s-d exchange coupling at the interface, μ_s relaxes by annihilating (generating) magnons in MI as μ_s has parallel (antiparallel) polarization to the magnetization of MI. The excited magnon current was thus manipulated by V_g: positive (negative) V_g increases (decreases) its magnitude. (b) Schematics of potential profile near the bottom NM-MI interface under positive V_g. (c) Schematics of probability $|\psi|^2$ at the bottom NM-MI interface under positive and negative V_g. (d) The predicted V_0 and E dependence of G_r (the color scale bar in units of $e^2/\hbar a^2$). (e) The E dependence of G_r under $V_0 = 5.625$, 5.675, and 5.725 eV extracted from Fig. 1(d).

bottom and top NM electrodes across the MI. V_g [Fig. 1(a)] across the NM-MI interface tilts downward (upward) the energy band of the MI [Fig. 1(b)], decreases (increases) the probability of electrons tunneling into the MI [Fig. 1(c)], and thus weakens (strengthens) the spin-magnon conversion efficiency at the interface and consequently changes the magnon excitation efficiency in the magnon transistor.

We extended the model by including the V_g-induced band bending of MI via the Hamiltonian

$$H_{\mathrm{MI}} = p^2/2m + V_0 + \Gamma\mathbf{S} \cdot \boldsymbol{\sigma} + ezV_g/t, \qquad (1)$$

where V_0 is the energy barrier at the interface, $\Gamma\mathbf{S} \cdot \boldsymbol{\sigma}$ describes the s-d coupling of electron spins $\boldsymbol{\sigma}$ in NM with localized moments $\mathbf{S}$ in MI, ezV_g/t describes the conduction band bending by V_g, and t is the MI thickness (calculation details in Supplemental Material [37]). The predicted V_0 and electric field E ($E = V_g/t$) dependence of the real part of $G_{\uparrow\downarrow}$ (G_r) was plotted in Fig. 1(d) (taking Fermi energy of NM $\varepsilon = 5$ eV and s-d coupling strength $\Gamma = 0.5$ eV for the Pt-YIG interface [4]). The typical G_r-E curves at three V_0 values [Fig. 1(e)] suggest the positive V_g
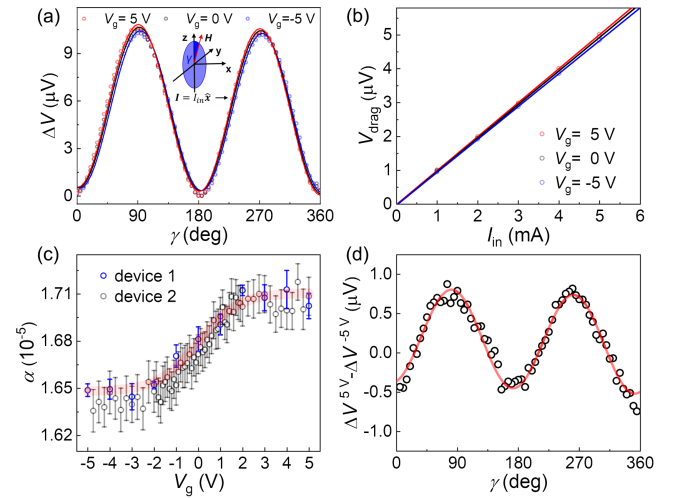

FIG. 2. Voltage-controlled MECD effect. (a) The γ dependence of ΔV with $\mathbf{H}$ rotated in the yoz plane and $I_{in} = 5$ mA under $V_g = -5$, 0, and $+5$ V. The open circles (solid lines) are the experimental data (fitted curves by $\Delta V = V_{drag}\cos 2\gamma$). (b) The I_{in} dependencies of V_{drag} under different V_g and their linear fittings. (c) The V_g dependence of magnon drag parameter α. Error bars for Devices 1 and 2 are from the standard deviations of the linear fittings of the V_{drag}-I_{in} relation and the $\Delta V = V_{drag}\cos 2\gamma$ fittings, respectively. The red line is the hyperbolic tangent fitting of the α-V_g curve. (d) The γ dependence of the difference in ΔV between $V_g = \pm 5$ V.

can efficiently increase G_r and vice versa. The spin-magnon convertance at the NM-MI interface is proportional to G_r [38] and thus the magnon current excited in MI can be modified by V_g as experimentally shown below.

The V_g-controlled magnon transistor was then experimentally achieved in a Pt(10)-YIG(80)-Pt(5 nm) sandwich in which V_g across YIG was able to tune the MECD effect. During measurements, the input current was applied on the bottom Pt (B-Pt) electrode alone $\hat{\mathbf{x}}$ direction, while the corresponding voltage (V) was detected on the top Pt (T-Pt) electrode along the same direction, the magnetic field was fixed at 1 T and rotated in the xoy, xoz, or yoz plane [see inset of Fig. 2(a)]. The measured V along the T-Pt electrode follows the following three characteristics (Fig. S6): (1) the angular dependence of the change in voltage (ΔV) picked up on the T-Pt electrode satisfying $\Delta V = V_{drag}\cos 2\theta$ (θ the angle between spin polarization $\boldsymbol{\sigma}$ and magnetization $\mathbf{M}$), (2) the linear dependence of V_{drag} on I_{in}, and (3) the $T^{5/2}$ temperature dependence, all coinciding with Refs. [7,8]. These features confirmed the MECD nature of the measured voltage. The insulating property of YIG was also checked by I_{leak}-V_g curves [Fig. S3(b)] with the leakage current being I_{leak}. I_{leak} was independent on $\mathbf{H}$, assuring the irrelevance of the observed $\mathbf{H}$-dependent V with I_{leak} (Fig. S4).

The V_g controllability of the MECD effect is clearly shown in Fig. 2. The MECD magnitude was noticeably

enhanced (weakened) under $V_g = +5$ V (-5 V) [Fig. 2(a)], which was further confirmed by the slope change of the V_{drag}-I_{in} curves [Fig. 2(b)]. The magnon drag parameter α was then calculated by $\alpha \equiv V_{drag}/(I_{in}R_{T\text{-}Pt})$. The V_g dependence of the extracted α [Fig. 2(c)] showed a clear change as $V_g = [-2$ V$, +2$ V$]$ and nearly saturated beyond the region. The maximum α tunability by V_g [defined by $\{[\alpha(V_g > +2$ V$) - \alpha(V_g < -2$ V$)]/\alpha(V_g < -2$ V$)\}$] reached $\sim 5\%$ with $\alpha(V_g > +2$ V$) \sim 1.71 \times 10^{-5}$ and $\alpha(V_g < -2$ V$) \sim 1.63 \times 10^{-5}$. The α controllability by V_g was also repeated in another Device 2 and many others. In order to trace the trend of the V_g-induced change in α, we fitted the α-V_g curve by a hyperbolic tangent function $\alpha = a + b \tanh(cV_g)$ as shown by the red line in Fig. 2(c). Note that this fitting only mathematically impacts with $|b/a|$ and c reflecting the magnitude and saturation speed of the V_g tunability, respectively. Here, for the α-V_g curve $|b/a| = 0.019$ and $c = -0.55$ V^{-1}.

In the following, we reveal the origin of the V_g tunability over the MECD effect. First, the V_g dependence of the MECD effect cannot be caused by any magnon coupling possibilities with the leakage current since I_{leak} increased divergently with the increase in $|V_g|$ and can be fitted by $I_{leak} = sgn(V_g)LV_g^2$ according to Mott-Gurney law [39], but α nearly saturated above ± 2 V. Second, the resistance of T-Pt directly changed by V_g was negligibly small ($< 0.008\%$, Fig. S8), also impossible to cause such significant change $\sim 5\%$ in the MECD (magnon mediated electric current drag) signal. Third, though negligibly small in garnets [40–42], the interfacial Dzyaloshinsky-Moriya interaction (DMI) may introduce an additional magnon-drift velocity $\mathbf{v}_{DMI} = \hat{\mathbf{z}} \times \hat{\mathbf{m}}(2\gamma D/M_s)$ to influence magnon transport with $\hat{\mathbf{z}}$ the interfacial normal, $\hat{\mathbf{m}}$ (M_s) the magnetization direction (saturated magnetization), γ the gyromagnetic ratio, and D a V_g-changeable parameter quantifying the DMI [43–45]. However, this DMI mechanism, if any, would bring about a 360° period in the yoz rotation owing to the $\hat{\mathbf{m}}$ dependence of $\mathbf{v}_{DMI}$. In stark contrast, the $\Delta V^{+5 \text{ V}} - \Delta V^{-5 \text{ V}}$ vs γ curve [Fig. 2(d)] shows a $\cos 2\gamma$ symmetry (180° period), thus ruling out the DMI origin of the V_g controllability.

To be more specific, the MECD effect can be explicitly expressed as below [4,6]:

$$\mathbf{j}_e^{T\text{-}Pt} \propto \theta_{SH}^{top}\theta_{SH}^{bottom}G_s^{s\text{-}m}G_s^{m\text{-}s}\boldsymbol{\sigma} \times (\mathbf{M} \times \mathbf{j}_e^{B\text{-}Pt}). \quad (2)$$

Here, $\mathbf{j}_e^{T\text{-}Pt}$ ($\mathbf{j}_e^{T\text{-}Pt}$) is the induced (input) charge current density along the T-Pt (B-Pt) electrode, $\theta_{SH}^{top(bottom)}$ is the spin Hall angle of the top (bottom) Pt electrode, $G_s^{s\text{-}m}(G_s^{m\text{-}s})$ is the effective spin-magnon (magnon-spin) convertance at the B-Pt–YIG (YIG–T-Pt) interface, $\boldsymbol{\sigma}$ is the spin polarization perpendicular to $\mathbf{j}_e^{T\text{-}Pt}$ and $\mathbf{M}$ is the YIG magnetization. Ruling out the above three reasons, the

MECD voltage can still be potentially manipulated by V_g in the following scenarios: (1) V_g-induced changes in the effective magnetization of YIG, (2) the spin Hall angles (θ_{SH}) of Pt, or (3) the spin-magnon conversion efficiency across the B-Pt–YIG or YIG–T-Pt interfaces. Hereafter, we experimentally check their possibilities one by one.

To investigate the V_g dependence of M_s, we conducted spin pumping experiments. The spin pumping voltage V_{SP} was picked up in the B-Pt electrode under various V_g as shown in Fig. 3(a). The H dependencies of a normalized V_{SP} at different f and V_g show no noticeable changes (variation $< 0.3\%$) in the resonance field (H_r) [Fig. 3(b)] and the overlapped Kittle fittings manifested no changes in the magnetization and anisotropy of YIG under V_g. Interestingly, the magnitude of V_{SP}^{peak} was changed by V_g [Fig. 3(c)]. The tunability defined by $\{[V_{SP}^{peak}(V_g = +3.9$ V$) - V_{SP}^{peak}(V_g = -3.9$ V$)]/V_{SP}^{peak}(V_g = -3.9$ V$)\}$ was also $\sim 5\%$. Moreover, the V_{SP}^{peak}-V_g tendency seemed similar to the V_{drag}-V_g relation, with $|b/a| = 0.021$ and $c = -0.54$ V^{-1} extracted from the hyperbolic tangent fitting [Fig. 3(g)]. We also tested V_{SP} along the T-Pt stripe, which had ideally identical H_r but opposite polarity with the B-Pt stripe [Fig. S7(a)]. However, V_{SP}^{peak} was not changed by V_g for the T-Pt detector [Fig. S7(c)]. Since spin currents were both pumped out from the sandwiched YIG, the different V_g controllability on V_{SP} for the B-Pt and the T-Pt detectors strongly hinted an interfacial gating origin instead of any bulk YIG reasons.

The following V_g-dependent spin Hall magnetoresistance (SMR) effect also supported this interfacial claim. For SMR measurement the resistance of the B-Pt electrode ($R_{B\text{-}Pt}$) was measured by four-terminal method with an 0.1 mA input current applied along $\hat{\mathbf{x}}$ direction and the sample rotated in the yoz plane in a 1 T magnetic field, as shown in Fig. 3(e). The angular dependence of the change in B-Pt resistance ($\Delta R_{B\text{-}Pt}$) was fitted by $\Delta R_{B\text{-}Pt} = R_{SMR} \cos 2\gamma$ and the SMR ratio was thus obtained by $|R_{SMR}/R_{B\text{-}Pt}|$. Since SMR originates from spin transfer at interfaces and is shunted by a thick Pt layer, we fabricated another Pt(4)-YIG(80)-Pt(5 nm) sandwich. Its $\Delta R_{B\text{-}Pt}$-γ relation at various V_g and the summarized V_g dependence of the SMR ratio are shown in Figs. 3(d) and 3(h). The similar coefficients of $|b/a| = 0.022$ and $c = -0.51$ V^{-1} were obtained from the hyperbolic tangent fitting [the red line in Fig. 3(h)], illustrating the V_g tunability on the SMR ratio also followed the similar trend as the V_g dependence of α and V_{SP}^{peak}. The SMR effect in the T-Pt stripe was independent on V_g [Figs. S7(b),(d)].

After the above analysis we have narrowed possibility for the V_g-controlled MECD effect to (1) a V_g-changeable spin Hall angle in B-Pt or (2) a V_g-controllable spin-magnon conversion efficiency across the B-Pt–YIG
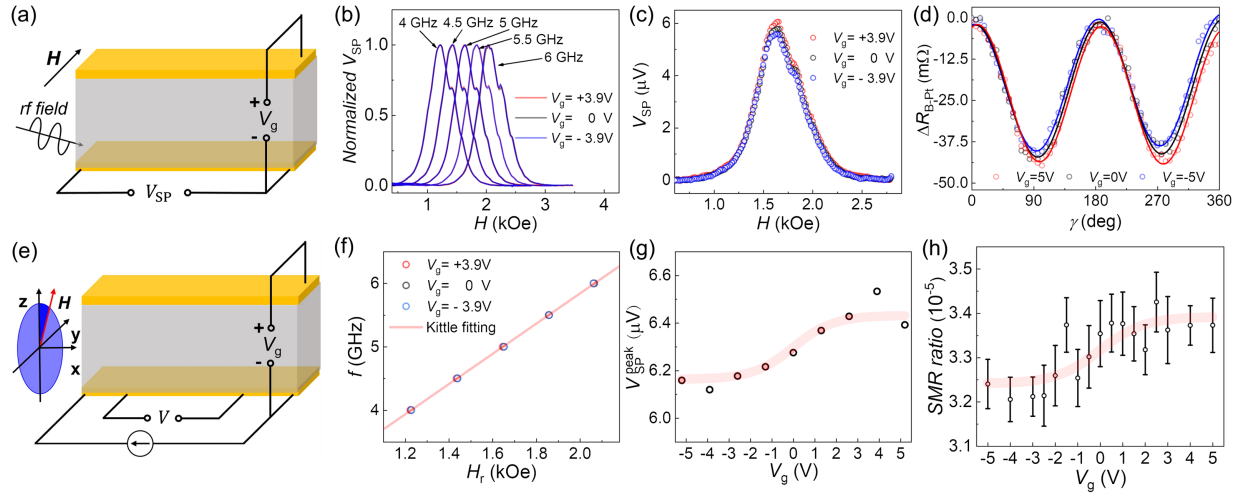
FIG. 3. Schematics setups for (a) spin pumping measurement where the spin pumping voltage (V_{SP}) was picked up along the B-Pt stripe with $\mathbf{H}$ perpendicular to the stripe and V_g applied across the sandwich and for (e) SMR measurement where the resistance change $\Delta R_{B\text{-Pt}}$ of the B-Pt stripe was measured with $\mathbf{H}$ rotated in the yoz plane. (b) The H dependence of the normalized $V_{SP}(H)/V_{SP}^{max}$ under different rf frequencies (f) and $V_g = -3.9$, 0, and $+3.9$ V. (c) The H dependence of V_{SP} at $f = 5$ GHz and $V_g = -3.9$, 0, and $+3.9$ V. (d) The γ dependencies of the $\Delta R_{B\text{-Pt}}$ (open circles) and their $\Delta R_{B\text{-Pt}} = \Delta R_{SMR} \cos 2\gamma$ fittings. (f) The resonance field (H_r) dependence of f under $V_g = -3.9$, 0, and $+3.9$ V (open circles) and their Kittle fittings. The V_g dependence of (g) the peak value of V_{SP}-H curve (V_{SP}^{peak}) under $f = 5$ GHz and (h) the SMR ratio. (Error bars from standard deviation of the $\Delta R_{B\text{-Pt}} = \Delta R_{SMR} \cos 2\gamma$ fittings.) Red lines in Figs. 3(c) and 3(d) are the hyperbolic tangent fitting of the V_{SP}^{peak}-V_g and SMR ratio-V_g curves, respectively.

interface. If the bulk spin Hall angle was modulated by V_g, we would not expect a substantial difference between the B-Pt and T-Pt stripes since they were both textured in the (111) orientation (Fig. S5). The V_g-independent resistivity of B-Pt (Fig. S8) did not support a V_g-modulated spin Hall angle of the B-Pt as well [46]. A voltage-tuned magnetic proximity effect in Pt may also cause a voltage dependence in the MECD signal; however, the unchanged anomalous Hall resistance (Fig. S8) has persuasively rule out this possibility.

We further measured the V_g-controlled MECD effect at different T. The V_g tunability over the MECD effect was strongly dependent on T from 240 to 300 K [Fig. 4(a)]. The difference in α under $V_g = \pm 5$ V increased by a factor of 3.5 (from 0.6×10^{-7} at 240 K to 2.1×10^{-7} at 300 K)

[Fig. 4(b)]. This strong T dependence cannot favor the possibility of a V_g-controlled intrinsic spin Hall conductivity (σ_{SH}^{int}) since the electronic structure of Pt varies little with T. Nevertheless, the strong T dependence can be naturally obtained as following. According to the spin-mixing conductance model across a NM-MI interface [4,6,35,36,47], the spin-torque-transfer efficiency and the spin-magnon convertance both depend on the s-d exchange coupling strength and thus probability of electrons penetrating into the insulating YIG as evanescent states. The probability certainly depends on the interface barrier (thus V_g) and also T, since T determines the kinetic energy of electrons in YIG. Supposing (1) ± 5 V gating leads to the similar band bending at different T and (2) the classic thermal activation theory holds, we would expect an
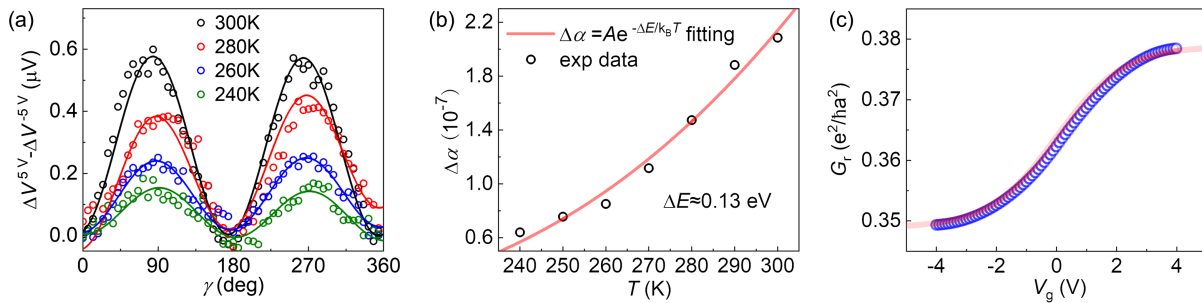

FIG. 4. (a) The γ dependence of $\Delta V(Vg = 5V) - \Delta V(Vg = -5V)$ under different T. (b) The T dependence of the difference in the magnon drag parameter $\Delta \alpha = \alpha(V_g = +5\text{ V}) - \alpha(V_g = -5\text{ V})$ between $V_g = \pm 5$ V. The solid lines are obtained by fitting data using $\Delta \alpha = A e^{-\Delta E/k_B T}$. (c) The calculated V_g dependence of G_r by taking redistributed voltage on the contact resistance ($R_{contact}$) into consideration. The red line is the hyperbolic tangent fitting result.

exponential T dependence (Arrhenius law [48]) for the MECD coefficient. Figure 4(b) shows the fitting well matched the experimental data and the caused difference in the effective tunneling barrier by $\pm V_g$ reached 0.13 eV. Since the spin-mixing conductance depended on the s-d coupling in the same way as the spin-magnon convertance, the SMR shared the same V_g dependence as the MECD effect naturally. Band bending at interfaces relies on charged defect density that pins the Fermi level and influences bending degree, which probably accounts for the observation that a smoother and well-crystallized B-Pt–YIG interface (evidenced by a sharper electron diffraction pattern at this region) contributed to the V_g controllability.

Now the above experimental data persuade us to attribute the V_g-controlled MECD effect to the V_g-induced changes in the spin-magnon convertance across the B-Pt–YIG interface. In theory, one would anticipate a monotonic change in spin-magnon conversion efficiency when an electric field is applied to the Pt-YIG interface [Fig. 1(e)]. This behavior had previously been observed in spin pumping experiments on YIG-Pt heterostructures with ionic gating [49,50]. However, the measured α-V_g deviated from the theoretical prediction by the saturation trend at large V_g. We attribute this deviation to the redistributed voltage on the contact resistance ($R_{contact}$) since I_{leak} increases divergently with V_g. In practice, we rewrote the Hamiltonian in YIG, considering the voltage dropped on $R_{contact}$ as follows:

$$H_{MI} = p^2/2m + V_0 + \Gamma \mathbf{S} \cdot \boldsymbol{\sigma} - \frac{ez}{t}(V_g - I_{leak}R_{contact}). \quad (3)$$

The calculated G_r-V_g relation [Fig. 4(c)] using parameters for Pt-YIG: Fermi energy $\varepsilon = 5$ eV, $V_0 = 5.5$ eV, $\Gamma = 0.5$ eV [4], and $R_{contact} = 15$ MΩ agrees well with experiment. G_r increased (decreased) with positive (negative) V_g and saturated at $V_g \approx \pm 2$ V. The calculated G_r change by V_g saturated at 13%/(MV/cm), also in a quantitative agreement with the experiment value ~10%/(MV/cm). The calculated result can also be well fitted with the hyperbolic tangent function with $|b/a| = 0.041$ and $c = -0.45$ V^{-1}. We fabricated magnon transistors with different junction areas and YIG thickness and obtained a systematic dependence of the modulation performances on the leakage current, which aligns well with numerical calculation results (Figs. S9–S12). This dependence promises that the voltage-controlled magnon transistors have chances of achieving a higher tunability at a higher saturation voltage by engineering a better interface with a lower leakage.

In summary we have experimentally demonstrated a field-effect magnon transistor based on the MECD effect in the Pt-YIG-Pt sandwich. With the voltage-induced band bending of YIG, the energy profile of the B-Pt–YIG interfacial barrier and consequently its spin-magnon convertance was modulated. In this sense, the MECD effect

was directly modulated by the gate voltage. Our finding promises direct modulation of spin-magnon conversion by electric fields, which shows a feasible pathway toward electrically controllable magnonics.

---

*Corresponding author: wancaihua@iphy.ac.cn
†Corresponding author: xfhan@iphy.ac.cn

[1] F. Bloch, Z. Phys. **61**, 206 (1930).
[2] A. Chumak, A. Serga, and B. Hillebrands, Nat. Commun. **5**, 4700 (2014).
[3] A. V. Chumak, V. Â. Vasyuchka, A. Â. Serga, and B. Hillebrands, Nat. Phys. **11**, 453 (2015).
[4] S. S.-L. Zhang and S. Zhang, Phys. Rev. Lett. **109**, 096603 (2012).
[5] S. S.-L. Zhang and S. Zhang, Phys. Rev. B **86**, 214424 (2012).
[6] S. M. Rezende, R. L. Rodríguez-Suárez, R. O. Cunha, A. R. Rodrigues, F. L. A. Machado, G. A. Fonseca Guerra, J. C. Lopez Ortiz, and A. Azevedo, Phys. Rev. B **89**, 014416 (2014).
[7] H. Wu, C. H. Wan, X. Zhang, Z. H. Yuan, Q. T. Zhang, J. Y. Qin, H. X. Wei, X. F. Han, and S. Zhang, Phys. Rev. B **93**, 060403(R) (2016).
[8] J. Li, Y. Xu, M. Aldosary, C. Tang, Z. Lin, S. Zhang, R. Lake, and J. Shi, Nat. Commun. **7**, 10858 (2016).
[9] K. Uchida, S. Takahashi, K. Harii, J. Ieda, W. Koshibae, K. Ando, S. Maekawa, and E. Saitoh, Nature (London) **455**, 778 (2008).
[10] O. Mosendz, J. E. Pearson, F. Y. Fradin, G. E. W. Bauer, S. D. Bader, and A. Hoffmann, Phys. Rev. Lett. **104**, 046601 (2010).
[11] L. J. Cornelissen, J. Liu, R. A. Duine, J. B. Youssef, and B. J. van Wees, Nat. Phys. **11**, 1022 (2015).
[12] L. J. Cornelissen and B. J. van Wees, Phys. Rev. B **93**, 020403(R) (2016).
[13] L. J. Cornelissen, J. Shan, and B. J. van Wees, Phys. Rev. B **94**, 180402(R) (2016).
[14] A. V. Chumak, A. A. Serga, M. B. Jungfleisch, R. Neb, D. A. Bozhko, V. S. Tiberkevich, and B. Hillebrands, Appl. Phys. Lett. **100**, 082405 (2012).
[15] Y. Onose, T. Ideue, H. Katsura, Y. Shiomi, N. Nagaosa, and Y. Tokura, Science **329**, 297 (2010).
[16] G. P. Zhang, W. Hübner, G. Lefkidis, Y. Bai, and T. F. George, Nat. Phys. **5**, 499 (2009).

[17] S. Murakami and A. Okamoto, J. Phys. Soc. Jpn. **86,** 011010 (2017).

[18] G. G. Siu, C. M. Lee, and Y. Liu, Phys. Rev. B **64,** 094421 (2001).

[19] H. Wu, L. Huang, C. Fang, B. S. Yang, C. H. Wan, G. Q. Yu, J. F. Feng, H. X. Wei, and X. F. Han, Phys. Rev. Lett. **120,** 097205 (2018).

[20] C. Y. Guo, C. H. Wan, X. Wang, C. Fang, P. Tang, W. J. Kong, M. K. Zhao, L. N. Jiang, B. S. Tao, G. Q. Yu, and X. F. Han, Phys. Rev. B **98,** 134426 (2018).

[21] C. Y. Guo, C. H. Wan, W. Q. He, M. K. Zhao, Z. R. Yan, Y. W. Xing, X. Wang, P. Tang, Y. Z. Liu, S. Zhang, Y. W. Liu, and X. F. Han, National electronics review **3,** 304 (2020).

[22] Z. R. Yan, C. H. Wan, and X. F. Han, Phys. Rev. Appl. **14,** 044053 (2020).

[23] C. Y. Guo, C. H. Wan, M. K. Zhao, H. Wu, C. Fang, Z. R. Yan, J. F. Feng, H. F. Liu, and X. F. Han, Appl. Phys. Lett. **114,** 192409 (2019).

[24] J. Cramer, F. Fuhrmann, U. Ritzmann, V. Gall, T. Niizeki, R. Ramos, Z. Qiu, D. Hou, T. Kikkawa, J. Sinova, U. Nowak, E. Saitoh, and M. Kläui, Nat. Commun. **9,** 1089 (2018).

[25] L. J. Cornelissen, J. Liu, B. J. van Wees, and R. A. Duine, Phys. Rev. Lett. **120,** 097702 (2018).

[26] G. Talmelli, T. Devolder, N. Träger, J. Förster, S. Wintz, M. Weigand, H. Stoll, M. Heyns, G. Schütz, I. P. Radu, J. Gräfe, F. Ciubotaru, and C. Adelmann, Sci. Adv. **6,** eabb4042 (2020).

[27] A. Haldar and A. O. Adeyeye, Appl. Phys. Lett. **116,** 162403 (2020).

[28] S. A. Chumak and A. Hillebrands, Nat. Commun. **5,** 4700 (2014).

[29] W. Yu, J. Lan, and J. Xiao, Phys. Rev. Appl. **13,** 024055 (2020).

[30] T. Seki, K. Utsumiya, Y. Nozaki, H. Imamura, and K. Takanashi, Nat. Commun. **4,** 1726 (2013).

[31] S. J. Hämäläinen, M. Madami, H. Qin, G. Gubbiotti, and S. van Dijken, Nat. Commun. **9,** 4853 (2018).

[32] J. Chen, H. Wang, T. Hula, C. Liu, S. Liu, T. Liu, H. Jia, Q. Song, C. Guo, Y. Zhang, J. Zhang, X. Han, D. Yu, M. Wu, H. Schultheiss, and H. Yu, Nano Lett. **21,** 6237 (2021).

[33] A. V. Sadovnikov, S. A. Odintsov, E. N. Beginin, S. E. Sheshukova, Y. P. Sharaevskii, and S. A. Nikitov, Phys. Rev. B **96,** 144428 (2017).

[34] H. Wang, M. Madami, J. Chen, H. Jia, Y. Zhang, R. Yuan, Y. Wang, W. He, L. Sheng, Y. Zhang, J. Wang, S. Liu, K. Shen, G. Yu, X. Han, D. Yu, J.-P. Ansermet, G. Gubbiotti, and H. Yu, Phys. Rev. X **13,** 021016 (2023).

[35] W. Chen, M. Sigrist, J. Sinova, and D. Manske, Phys. Rev. Lett. **115,** 217203 (2015).

[36] W. Chen, M. Sigrist, and D. Manske, Phys. Rev. B **94,** 104412 (2016).

[37] See Supplemental Material at http://link.aps.org/supplemental/10.1103/PhysRevLett.132.076701 for details in numerical calculation of voltage controlled spin mixing conductance, material characterization of magnon transistors, experimental evidences for voltage uncontrollability of top Pt/YIG interface, magnon transistors with different geometry and leakage current dependence of tunability and saturation electric field.

[38] L. J. Cornelissen, K. J. H. Peters, G. E. W. Bauer, R. A. Duine, and B. J. van Wees, Phys. Rev. B **94,** 014412 (2016).

[39] N. F. Mott and R. W. Gurney, *Electronic Processes in Ionic Crystals*, 2nd ed. (Dover Publication, Inc., New York, 1964).

[40] C. O. Avci, E. Rosenberg, L. Caretta, F. Büttner, M. Mann, C. Marcus, D. Bono, C. A. Ross, and G. S. D. Beach, Nat. Nanotechnol. **14,** 561 (2019).

[41] S. Vélez, J. Schaab, M. S. Wörnle, M. Müller, E. Gradauskaite, P. Welter, C. Gutgsell, C. Nistor, C. L. Degen, M. Trassin, M. Fiebig, and P. Gambardella, Nat. Commun. **10,** 4750 (2019).

[42] S. Ding, A. Ross, R. Lebrun, S. Becker, K. Lee, I. Boventer, S. Das, Y. Kurokawa, S. Gupta, J. Yang, G. Jakob, and M. Kläui, Phys. Rev. B **100,** 100406(R) (2019).

[43] H. Wang, J. Chen, T. Liu, J. Zhang, K. Baumgaertl, C. Guo, Y. Li, C. Liu, P. Che, S. Tu, S. Liu, P. Gao, X. Han, D. Yu, M. Wu, D. Grundler, and H. Yu, Phys. Rev. Lett. **124,** 027203 (2020).

[44] P. Fan, Z. H. Zheng, Z. K. Cai, T. B. Chen, P. J. Liu, X. M. Cai, D. P. Zhang, G. X. Liang, and J. T. Luo, Appl. Phys. Lett. **102,** 033904 (2013).

[45] H. T. Nembach, J. M. Shaw, M. Weiler, E. Jué, and T. J. Silva, Nat. Phys. **11,** 825 (2015).

[46] S. Dushenko, M. Hokazono, K. Nakamura, Y. Ando, T. Shinjo, and M. Shiraishi, Nat. Commun. **9,** 3118 (2018).

[47] S. Ok, W. Chen, M. Sigrist, and D. Manske, J. Phys. Condens. Matter **29,** 075802 (2016).

[48] A. K. Galwey and M. E. Brown, Thermochim. Acta **386,** 91 (2002).

[49] S.-J. Xu, X. Fan, S.-M. Zhou, X. Qiu, and Z. Shi, J. Phys. D **52,** 175304 (2019).

[50] L. Wang, Z. Lu, J. Xue, P. Shi, Y. Tian, Y. Chen, S. Yan, L. Bai, and M. Harder, Phys. Rev. Appl. **11,** 044060 (2019).